

# Fano-like resonances sustained by Si doped InAsSb plasmonic resonators integrated in GaSb matrix

Thierry Taliercio,<sup>1,2,\*</sup> Vilianne NTsame Guilengui,<sup>1,2</sup> Laurent Cerutti,<sup>1,2</sup>  
Jean-Baptiste Rodriguez,<sup>1,2</sup> Franziska Barho,<sup>1,2</sup> Maria-José Milla Rodrigo,<sup>1,2</sup>  
Fernando Gonzalez-Posada,<sup>1,2</sup> Eric Tournié,<sup>1,2</sup> Michael Niehle,<sup>3</sup> and Achim Trampert<sup>3</sup>

<sup>1</sup>Univ. Montpellier, IES, UMR 5214, F-34000, Montpellier, France

<sup>2</sup>CNRS, IES, UMR 5214, F-34000, Montpellier, France

<sup>3</sup>Paul-Drude-Institut für Festkörperelektronik, D-10117 Berlin, Germany

\*[thierry.taliercio@umontpellier.fr](mailto:thierry.taliercio@umontpellier.fr)

**Abstract:** By using metal-free plasmonics, we report on the excitation of Fano-like resonances in the mid-infrared where the Fano asymmetric parameter,  $q$ , varies when the dielectric environment of the plasmonic resonator changes. We use silicon doped InAsSb alloy deposited by molecular beam epitaxy on GaSb substrate to realize the plasmonic resonators exclusively based on semiconductors. We first demonstrate the possibility to realize high quality samples of embedded InAsSb plasmonic resonators into GaSb host using regrowth technique. The high crystalline quality of the deposited structure is confirmed by scanning transmission electron microscopy (STEM) observation. Second, we report Fano-like resonances associated to localized surface plasmons in both cases: uncovered and covered plasmonic resonators, demonstrating a strong line shape modification. The optical properties of the embedded structures correspond to those modeled by finite-difference time-domain (FDTD) method and by a model based on Fano-like line shape. Our results show that all-semiconductor plasmonics gives the opportunity to build new plasmonic structures with embedded resonators of highly doped semiconductor in a matrix of un-doped semiconductor for mid-IR applications.

©2015 Optical Society of America

**OCIS codes:** (050.2770) Gratings; (240.6680) Surface plasmons; (260.3910) Metals optics; (310.6860) Thin films, optical properties;

---

## References and links

1. A. Pors, M. G. Nielsen, T. Bernardin, J.-C. Weeber, and S. I. Bozhevolnyi, "Efficient unidirectional polarization-controlled excitation of surface plasmon polaritons," *Sci. Appl.* **3**(8), e197 (2014).
2. N. Yu, R. Blanchard, J. Fan, F. Capasso, T. Edamura, M. Yamanishi, and H. Kan, "Small divergence edge-emitting semiconductor lasers with two-dimensional plasmonic collimators," *Appl. Phys. Lett.* **93**(18), 181101 (2008).
3. S. Collin, G. Vincent, R. Haïdar, N. Bardou, S. Rommeluère, and J.-L. Pelouard, "Nearly Perfect Fano Transmission Resonances through Nanoslits Drilled in a Metallic Membrane," *Phys. Rev. Lett.* **104**(2), 027401 (2010).
4. G. V. Naik, V. M. Shalaev, and A. Boltasseva, "Alternative Plasmonic Materials: Beyond Gold and Silver," *Adv. Mater.* **25**(24), 3264–3294 (2013).
5. D. Li and C. Z. Ning, "All-semiconductor active plasmonic system in mid-infrared wavelengths," *Opt. Express* **19**(15), 14594–14603 (2011).
6. E. Tokumitsu, "Correlation between Fermi Level Stabilization Positions and Maximum Free Carrier Concentrations in III–V Compound Semiconductors," *Jpn. J. Appl. Phys.* **29**(2), L698–L701 (1990).
7. T. Taliercio, V. Ntsame Guilengui, L. Cerutti, J.-B. Rodriguez, and E. Tournié, "GaSb-based all-semiconductor mid-IR plasmonics," *Proc. SPIE* **8631**, 8631–8672 (2013).
8. I. Vurgaftman, J. R. Meyer, and L. R. Ram-Mohan, "Band parameters for III–V compound semiconductors and their alloys," *J. Appl. Phys.* **89**(11), 5815 (2001).

9. T. Taliercio, V. Ntsame Guilengui, L. Cerutti, E. Tournié, and J.-J. Greffet, "Brewster "mode" in highly doped semiconductor layers: an easy way to measure the plasma frequency of thin layers," *Opt. Express* **22**(20), 24294–24303 (2014).
10. S. J. Pearton and D. R. Norton, "Dry etching of electronic oxides, polymers, and semiconductors," *Plasma Process. Polym.* **2**(1), 16–37 (2005).
11. C. Constantine, D. Johnson, S. J. Pearton, U. K. Chakrabarti, A. B. Emerson, W. S. Hobson, and A. P. Kinsella, "Plasma etching of III–V semiconductors in CH<sub>4</sub>/H<sub>2</sub>/Ar electron cyclotron resonance discharges," *J. Vac. Sci. Technol. B* **8**(4), 596 (1990).
12. V. N'Tsame Guilengui, L. Cerutti, J.-B. Rodriguez, E. Tournié, and T. Taliercio, "Localized surface plasmon resonances in highly doped semiconductors nanostructures," *Appl. Phys. Lett.* **101**(16), 161113 (2012).
13. S. A. Maier, *Plasmonics: Fundamentals and Applications* (Springer, 2007), Chap. 5.
14. J. Leon and T. Taliercio, "Large tunable photonic band gaps in nanostructured doped semiconductors," *Phys. Rev. B* **82**(19), 195301 (2010).
15. E. D. Pauk, and R. T. Holm, "Indium Arsenide (InAs)," in *Handbook of Optical Constants of Solids*, E. D. Palik, ed. (Academic, 1985).
16. B. R. Bennett, R. A. Soref, and J. A. del Alamo, "Carrier-Induced Change in Refractive Index of InP, GaAs, and InGaAsP," *J. Quant. Electron.* **26**(1), 113–122 (1990).
17. D. F. Edwards, and R. H. White, "Gallium Antimonide (GaSb)," in *Handbook of Optical Constants of Solids*, E. D. Palik, ed. (Academic, 1985).
18. A. E. Miroshnichenko, S. Flach, and Y. S. Kivshar, "Fano resonances in nanoscale structures," *Rev. Mod. Phys.* **82**(3), 2257–2298 (2010).
19. Finite difference time domain method has been done with Lumerical FDTD Solutions from Lumerical Solutions Inc.

---

## 1. Introduction

Plasmonics offers the possibility to integrate new optical functionalities including, polarization control [1], beaming [2], filtering [3] among others, in photonic circuits or in photonic devices. The strong field enhancement obtained at nanometric scale in metallic nanostructures, enables developing new nanophotonics functionalities with plasmonic systems. Au and much more occasionally Ag are the mostly used materials to demonstrate these potential applications. Unfortunately, even if these materials are ideal for plasmonics, they have several drawbacks. Au is CMOS incompatible which is an inhibiting point for potential industrial application and Ag is unstable, it oxidizes. Thus, it is strongly required to find alternative materials to develop industrial applications based on plasmonics [4]. Recently, a few works have demonstrated [5] the possibility to realize highly integrated plasmonic circuits exclusively using semiconductors.

In this work, we demonstrate the possibility to develop all semiconductor plasmonics by realizing a highly Si-doped InAsSb array supporting localized surface plasmon resonances (LSPR), embedded into GaSb, a common semiconductor of mid-infrared photonics. Depending on the matrix material we observe Fano-like resonances in these all-semiconductor plasmonic resonators. Besides, we demonstrate the successful development of building blocks needed to integrate a plasmonic functionality into a photonic device.

We have chosen to work with InAsSb alloys because of their specific physical properties. First, InAs<sub>0.91</sub>Sb<sub>0.09</sub> is lattice matched to GaSb substrate guaranteeing the high structural quality of the samples. Second, InAs<sub>0.91</sub>Sb<sub>0.09</sub> is one the easiest materials to dope [6] and has a band alignment avoiding carrier transfer to juxtaposed un-doped GaSb semiconductor [7]. Finally, the small effective mass of InAsSb alloys [8] allows reaching a high plasma frequency which is proportional to the inverse of the square root of the effective mass.

## 2. Samples: InAsSb arrays on GaSb

The samples consist of Si doped InAs<sub>0.91</sub>Sb<sub>0.09</sub> layers grown by molecular beam epitaxy (MBE) on doped GaSb lattice matched substrates ( $1\text{--}2 \cdot 10^{18} \text{ cm}^{-3}$ ). The thickness of the layers is 100 nm (Fig. 1-a). The carrier density in this thin layer is controlled by the optical technique recently developed and based on the Brewster mode [9]. The Brewster mode is a leaky mode appearing near the plasma frequency,  $\omega_p$ . The Brewster mode and Brewster angle refer to the same behavior which is to suppress reflected beam under *p*-polarized light.

However, in the case of the Brewster mode, due to the fact that the permittivity,  $\epsilon$ , tends to zero a field enhancement appears provoking absorption at a given frequency on a large range of angles. The typical carrier density of the samples, obtained via Brewster mode measurements, is  $n = 3.4 \cdot 10^{19} \text{ cm}^{-3}$  and corresponds to a plasma wavenumber,  $\nu_p$ , around  $0.16 \mu\text{m}^{-1}$  or a plasma wavelength,  $\lambda_p$ , of  $6.25 \mu\text{m}$ . Samples A and B are from the same wafer. The sample C is the sample B after regrowth of a thin layer of GaSb.

The technological process to fabricate the plasmonic arrays is represented in Fig. 1. After deposition of a  $\text{SiO}_2$  mask (Fig. 1(b)), a holographic insolation is realized using AZMIR 701 diluted positive photoresist (Fig. 1(c)).

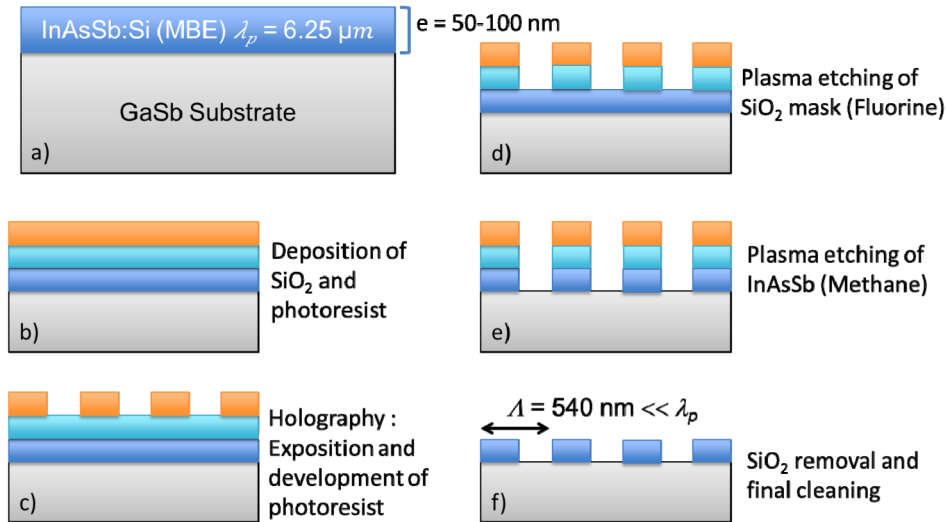


Fig. 1. Steps of the technological process of the studied samples. a) MBE growth of the InAsSb:Si layer on a GaSb substrate. b)  $\text{SiO}_2$  deposition and photoresist (AZMIR701) spin-coating. c) Holographic insolation and development of the photoresist. d) ICP-RIE of the  $\text{SiO}_2$  mask performed with  $\text{CHF}_3:\text{O}_2$  recipe. e) ICP-RIE of the InAsSb:Si mask performed with  $\text{Cl}_2:\text{N}_2:\text{Ar}$  recipe. f) Final cleaning and  $\text{SiO}_2$  removal.

We used a two steps dry etching process. First, we used inductively-coupled plasma reactive ion etching (ICP-RIE) with a  $\text{CHF}_3:\text{O}_2$  recipe [10] for the  $\text{SiO}_2$  mask etching (Fig. 1(d)). Second, we used ICP-RIE with a  $\text{Cl}_2:\text{N}_2:\text{Ar}$  recipe [11] to etch the InAsSb layer (Fig. 1(e)). Finally, we removed the photoresist and  $\text{SiO}_2$  mask using a  $\text{HF}:\text{H}_2\text{O}$  solution (Fig. 1(f)). The periodicity ( $\Delta$ ) of the array and the typical ribbon width are respectively 540 nm and 240 nm for all samples studied in this article. To obtain complementary data from sample fabrication see [12].

### 3. Localized surface plasmon resonances in InAsSb arrays

The samples have been characterized by angular reflectance measurements. The experimental setup is a Nicolet NEXUS 870 Fourier transform infrared (FTIR) spectrometer. A KBr beam splitter and DTGS detector are used to work in the infrared range between  $350 \text{ cm}^{-1}$  and  $7400 \text{ cm}^{-1}$ . Reflectance measurements have been performed varying the incidence angle for  $s$  (electric field along the ribbons) and  $p$  (electric field perpendicular to the ribbons) polarizations. Changing the polarization and the incidence angle allowed identifying surface plasmon modes. The angular dependent reflectance setup is coupled to the FTIR and consists of gold mirrors mounted on two arms rotating around the optical axis. It gives access to angles from  $0^\circ$  up to  $84^\circ$ . To polarize the incident light, a KRS holographic wire grid polarizer has been used. Finally a diaphragm allows controlling the angular aperture of the setup at  $\pm 0.5^\circ$ . Dispersion relations are obtained by gathering spectra taken each  $4^\circ$ . Each reflectance

spectrum, such as the one displayed in Fig. 2, is an average of 2000 spectra using a gold film deposited on a GaSb substrate as reference. To build the reflectance dispersion of Fig. 3, it was necessary to interpolate numerical values between the experimental values because the relation between wavenumbers,  $\nu$ , and wavevectors,  $k$ , is not linear:

$$\nu = \frac{k}{2\pi} \sin(\theta) \quad (1)$$

where  $\theta$  is the angle of incidence of light. Before the interpolation procedure, we have numerically smoothed the experimental values to reduce the amplitude fluctuations between each spectrum. A two-dimensional matrix is then generated with wavevectors in  $x$ , wavelength in  $y$  and reflectance intensity in  $z$ .

Figure 2 shows the reflectance spectrum of sample A obtained in normal incidence under p-polarized light. The plasma wavenumber,  $\nu_p$ , and wavelength,  $\lambda_p$ , are indicated by the vertical black arrows respectively at  $0.16 \mu\text{m}^{-1}$  and  $6.25 \mu\text{m}$ .

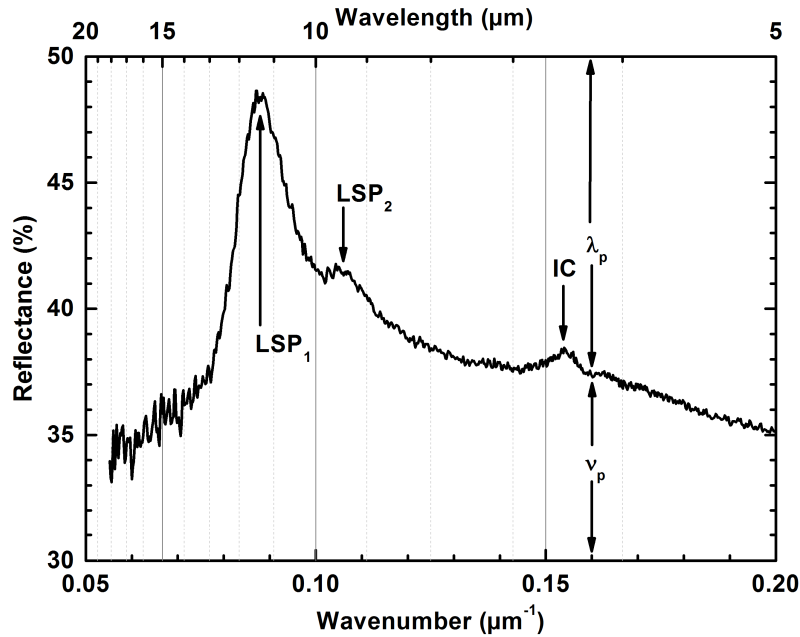


Fig. 2. Reflectance spectra of the sample A obtained in normal incidence under p-polarized light.  $\nu_p$  and  $\lambda_p$  correspond respectively to the plasma wavenumber and plasma wavelength. LSP and IC correspond respectively to localized surface plasmons mode and ionic crystal like behavior.

Three plasmonic modes can be identified respectively at  $0.088 \mu\text{m}^{-1}$ ,  $0.105 \mu\text{m}^{-1}$  and  $0.154 \mu\text{m}^{-1}$ . The two modes at low wavenumbers are related to the surface plasmon which exists at the interface between the InAsSb ribbons and the GaSb substrate. Generally speaking, surface plasmon polaritons are associated to metallic gratings. However, since the grating periodicity is extremely small compared to  $\lambda_p$  (see Fig. 1(f)), the two modes labelled LSP can be defined as localized surface plasmons [13]. Indeed, they can be viewed either as large wavevector surface plasmons or as coupled localized surface plasmons. But in each case the localized nature of the surface plasmon is established. The ribbons width is typically 240 nm which is 30-times smaller than  $\lambda_p$ . They are comparable to gold nanorods of less than 10 nm that support localized surface plasmon resonances. Finally, these resonances are extremely sensitive to the ribbon width [12]. The last mode labelled IC, for ionic crystal is associated to localized surface plasmon modes between ribbons. The grating can be modeled by a

homogenized material behaving as an ionic crystal [14]. For a thick enough InAsSb layer Fabry-Perot modes can be supported by this homogenized material but at smaller wavenumber. To confirm the localized nature of the modes we performed angular-dependent reflectance measurements.

The reflectance dispersion of Fig. 3 shows the spectral signature of the Brewster mode at  $0.16 \mu\text{m}^{-1}$ . It can be also observed a minimum of reflectance along the light cone (black dashed line) which corresponds to the Brewster angle of the InAsSb layer. The corresponding angle,  $71^\circ \pm 1^\circ$ , allows to extract the value of the refractive index  $\eta = 2.9 \pm 0.15$ .

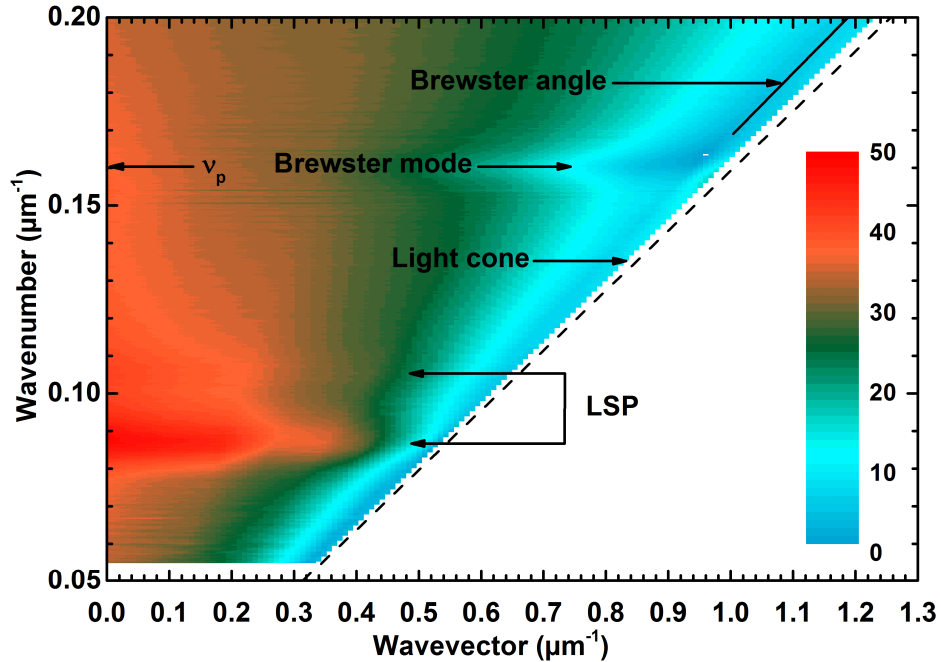


Fig. 3. Reflectance dispersion under  $p$ -polarized light of sample A. The light cone is represented by the dark dashed line. The Brewster angle is represented by the dark line and the Brewster mode is indicated by the horizontal arrows. The associated plasma wavenumber is indicated on the y axis. The surface plasmon polariton modes are indicated by the linked arrows.

This value is smaller than those gathered in the literature, 3.5 at a wavelength of  $4 \mu\text{m}$  [15]. This difference is mainly attributed to the free carrier density [16]. Indeed, the free carriers provoke an index variation  $\Delta\eta$  as:

$$\Delta\eta = \frac{-6.9 \times 10^{-22}}{\eta(\hbar\omega)^2} \left\{ n \left( \frac{m_0}{m_e} \right) \right\}, \quad (2)$$

where,  $m_e$  and  $m_0$  are respectively the electron effective mass, the electron mass in vacuum,  $\hbar$  is the Planck constant and  $\omega$  the angular frequency. The fundamental constants have been used.  $\hbar\omega$  and  $n$  (carrier density) are expressed in eV and in  $\text{cm}^{-3}$  respectively. Taking into account that the effective masse varies with the doping level ( $0.1 m_0$  for  $n = 3.4 \cdot 10^{19} \text{cm}^{-3}$ ) we obtain an index variation of  $-0.7$ . The expected value of  $\eta$  is then 2.8 which is coherent with the measured value.

Figure 3 also shows the two main plasmonic modes at  $0.088 \mu\text{m}^{-1}$  and  $0.105 \mu\text{m}^{-1}$ . They do not shift when the wavevector or the angle of incidence varies. This is an experimental

demonstration that these modes correspond to localized surface plasmons. The behavior of the IC mode at  $0.154 \mu\text{m}^{-1}$  is visible in Fig. 3, but not at high angles.

#### 4. Embedded InAsSb arrays into GaSb: epitaxial regrowth

To reach the integration of the plasmonic functionality at the heart of the photonic devices, it is necessary to control the epitaxial regrowth of a capping layer of GaSb keeping constant the crystalline quality of the material. To ensure the optimal growth conditions, we developed an accurate cleaning process. We use an  $\text{O}_2$  plasma to remove all traces of the photoresist and a  $\text{HF}:\text{H}_2\text{O}$  (1:10) bath to remove the  $\text{SiO}_2$  mask.

Once the samples are cleaned we reload them in the MBE to complete the structure with 500 nm of GaSb. To check the crystalline quality of the regrowth we performed a transmission electron microscopy (TEM) investigation using a JEOL 2100F microscope operating at 200 kV. Cross-sections through the InAsSb ribbons have been prepared by focused ion beam sample preparation with a JEOL 4501 FIB/SEM dual beam device. The lift-out technique is applied to extract a TEM lamella for the analysis of the ribbon morphology and microstructure. The FIB preparation allows obtaining large plan-parallel areas of the region of interest. Figure 4 represents bright-field scanning TEM (BF STEM) images of the cross-section specimen of sample C. The sample is viewed along a  $[110]$  direction. These imaging conditions are sensitive to the presence of threading dislocations or stacking faults. It has been found that the regrown GaSb layer is nearly free of crystal defects. The array periodicity is 535 nm and the capping layer thickness is 500 nm. We can see that the top surface is perfectly flat, a prerequisite to envisage integrating plasmonic functionalities into photonic devices.

The ribbon side walls appear oblique and the thin dark line between contiguous ribbons is the consequence of the under-etching. This dark line is probably related to an InAs layer redeposited during the etching process.

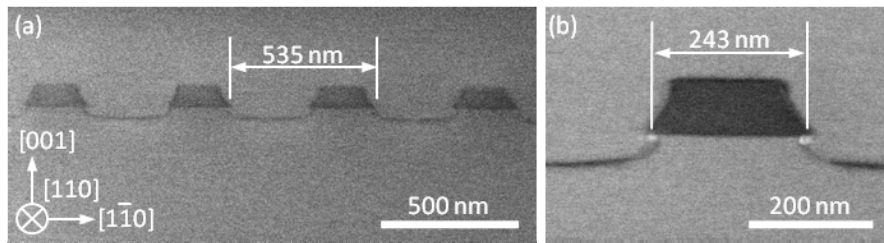


Fig. 4. Bright-Field Scanning transmission electron microscopy (BF STEM) of the sample C. a) general cross section, b) zoom of the cross section of one ribbon.

Figure 4(b) is a BF STEM picture of one InAsSb:Si ribbon. One can clearly see that the ribbons do not have vertical side walls and that they are not exactly oblique. White spots are seen below the bottom corner of the ribbons which are small voids all along the ribbons. We have considered this specific shape in the FDTD simulation. It is noticeable that the shape of the InAsSb:Si ribbons does not induce the generation of extended defects that thread through the GaSb capping layer. This is a demonstration of our control of the surface quality and the epitaxial regrowth.

#### 5. Results and discussion: Fano-like resonances observation

Samples of the same wafer before (sample B) and after (sample C) MBE regrowth have been studied by reflectance measurements under normal incidence (Fig. 5) and by angular-dependent measurements.

The angular-dependent reflectance results were similar for all the samples of the same wafer and demonstrated the localized origin of the observed resonances (see Fig. 3). In Fig. 5, the reflectance spectra in dark shows the two LSP modes and the IC mode (vertical black

arrows) which are sustained by the InAsSb:Si array. When the array is covered by the GaSb capping layer (red dashed curve) the resonances are red-shifted and completely reshaped. The red-shift is due to the modification of the ribbon environment: the refractive index at the top corner of the ribbon varies from 1 to 3.71-3.74 [17], the GaSb refractive index. The shape modification is much more surprising and looks like a Fano shape resonance.

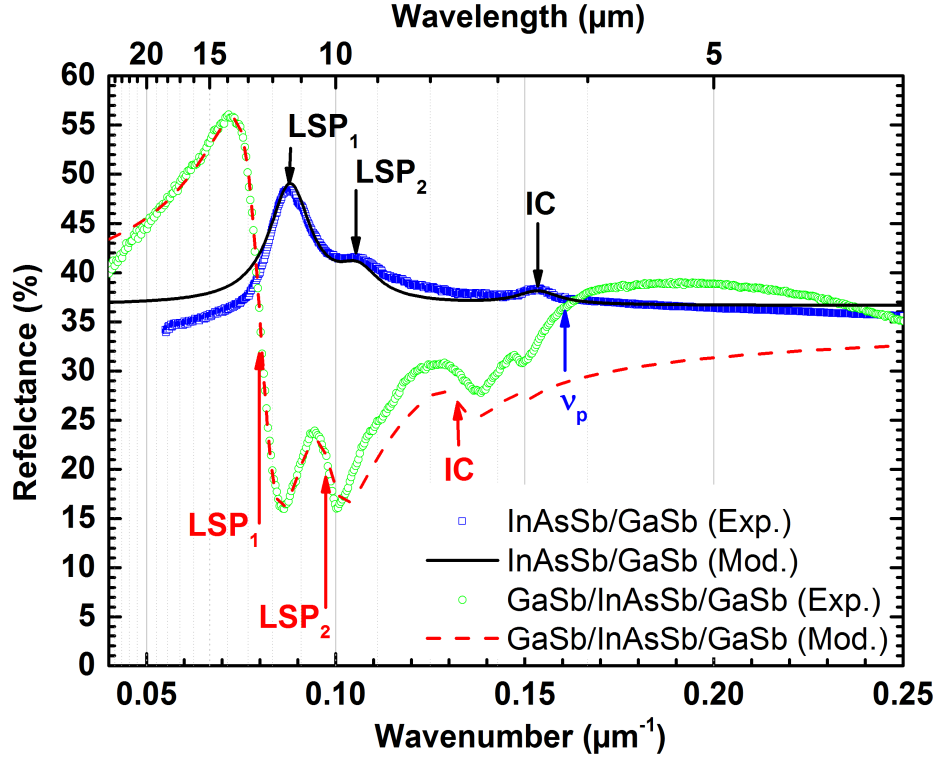


Fig. 5. Reflectance spectra of the samples B and C. The blue open squares and green open circles correspond respectively to the experimental results of the samples B and C. Dark and red dashed lines correspond respectively to model using Fano-like scattering function of the samples B and C. The labels landmark the different localized plasmon modes  $LSP_i$  ( $i = 1, 2$ ), IC and the plasma wavenumber,  $v_p$ .

Fano resonances appear when interferences exist between a continuum of states (broad band width) and discrete states (narrow band width). They appear as narrow band in the spectrum, which in general has the form:

$$F(\Omega) = \frac{(\Omega + q)^2}{(\Omega^2 + 1)}, \quad (3)$$

with

$$\Omega = \frac{(\omega - \omega_{LSP})}{\gamma_{LSP} / 2}, \quad (4)$$

where  $\omega_{LSP}$  is the frequency of LSP or IC resonance,  $\gamma_{LSP}$  is the spectral width of the LSP or IC resonance and  $q$  is the Fano asymmetry parameter.

We fitted the reflectance spectra of sample B (before regrowth). Because we work under reflectance configuration we do not obtain a dip but a rise in the spectra. To calculate the reflectance from the transmittance we use the relation  $R = 1 - T$ . So, we do not consider

absorbance that can explain the weak differences between the experimental and simulation results. Each plasmonic resonance is taken independently and is multiplied by a coefficient to adjust the strength of the resonance. We keep constant  $\gamma_{LSP}$  ( $0.0034\mu\text{m}^{-1}$ ) and adjust the frequencies of the different LSP resonances.  $q$  is calculated to be close to 0.01. This can be explained because the resonators provoke destructive interferences with the background. Part of the light is reflected, depending of the strength of the plasmonic resonance. The Fano asymmetric factor equal to 0 signifies that the dominating path is the scattering process from discrete states [18]. In our system, these discrete states are the localized plasmonic modes, LSP. They are characterized by a narrow band width. The continuum of states is the direct transmitted light through the homogenized material, that is, the InAsSb grating [14]. The homogenized material supports surface plasmon polaritons (SPP) with very large wavevectors [3]. When the refractive indexes at each interface of the homogenized material are different, the strong impedance mismatch weakened the direct transmitted light. This favors discrete states path compared to the continuum states path. The Fano asymmetric factor tends to 0. The line shape is symmetric.

The situation is completely different for the buried grating. Indeed, the refractive indexes at each interface of the homogenized material are then equals. The coupling to the continuum states is strengthened. This path becomes efficient. For the regrown sample (sample C),  $q$  is close to unity, 1.2, which denotes the fact that directly transmitted light through the grating (homogenized material) and the scattered light by the plasmonic resonators have the same strength leading to interferences. Because of the phase variation in energy of the plasmonic resonance, an asymmetric line shape is obtained for each resonance. The spectral widths kept constant. The Fano-model still works but it requires the addition of a fourth resonance at  $0.15\mu\text{m}^{-1}$ . To validate our approach we compare the Fano-model to the FDTD simulations before and after the regrowth by using the exact shape and geometry measured in Fig. 4 [19].

For the FDTD simulation we used a Drude function to model the InAsSb:Si material and a dynamic dielectric constant for GaSb equal to  $\epsilon_{GaSb} = 3.72$  [17]. For InAsSb:Si we used  $\nu_p = 0.16\mu\text{m}^{-1}$ ,  $\gamma = 0.01 \times \nu_p$  and  $\epsilon_\infty = 11.7$  [15]. The FDTD simulations are represented in Fig. 6(a) and Fig. 6(b) respectively for the sample before (Sample B) and after (sample C) the regrowth. The dark curves correspond to the reflectance spectra (left vertical axis) of the samples, whereas red curves correspond to scattering cross-section spectra (right vertical axis) of individual ribbons. The specific shape of the InAsSb:Si ribbons was taken under consideration. The general aspect of the FDTD spectra resembles this of the Fano-model in Fig. 5. To validate the Fano-like behavior of our samples we have compared the scattering cross-section spectra with reflectance spectra. In the case of InAsSb:Sb gratings on GaSb substrate both spectra are similar (Fig. 6(a)). They have same shape, same peak energies. First, this demonstrates that the coupling between ribbons is negligible, and, second, the reflectance spectra are dominated by the discrete states path associated to the localized surface plasmons.

Simulations of the electric profiles of the ribbons have been done in relation to the geometrical shape, as described in [12]. In the simulation, the oblique side wall and under-etching effect have been taken into account as represented in the electric field profile of Fig. 6 by the white line. Measurements of the shapes and dimensions of the ribbons are further given in Fig. 4.

The electric field profiles of the modes are shown in the insets and indicated on the spectra by the arrows (Fig. 6(a)). The mode at higher wavenumber, IC, is mainly pinned at the top corners of the ribbons but extends also to the bottom corner. It corresponds to the surface plasmons existing at the lateral interfaces between the InAsSb ribbons. Their localized origin is due to the thin thickness of the InAsSb layer, 100 nm.

The electric field profiles of the  $LSP_i$  modes show a strong field enhancement at the bottom corner (Fig. 6(a)). These modes are pinned at the bottom interface between

InAsSb/GaSb and correspond to dipolar-like modes. The complexity of the geometry of the ribbons allows sustaining few dipolar modes.

In the case of the buried InAsSb grating, Fig. 6(b), the scattering cross-section spectrum (red line) is red-shifted as expected but does not change its shape compared to the InAsSb grating on the GaSb substrate except a strengthening of the IC. This strengthening can be easily understood in terms of strong coupling enhancement due to the permittivity increase, 1 to 13.8, of the un-doped semiconductor. See [14] for more details.

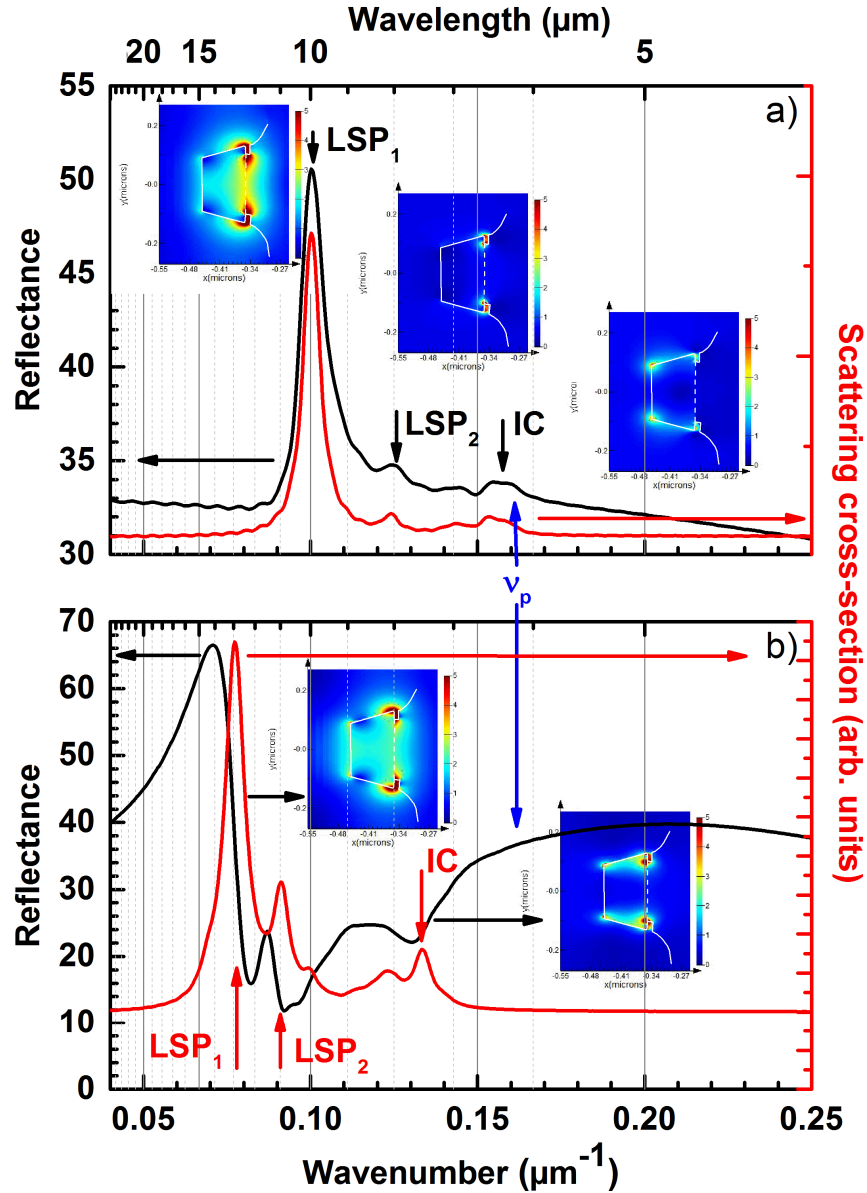


Fig. 6. Simulation of the reflectance spectra (dark curve, left axis) and the scattering cross-section (red curve, right axis) of a) the sample B and b) the sample C via the FDTD method. The labels landmark the different localized plasmon modes  $LSP_i$  ( $i = 1, 2$ ), IC and the plasma wavenumber,  $v_p$ . The insets correspond to the electric field profile of the plasmonic modes pointed by the arrows. The white lines correspond to the shape of the ribbons. The white dashed lines correspond to the InAsSb/GaSb interfaces.

The associated resonances to LSP are centered to Fano-like resonances observed in the reflectance spectrum (dark line). The electric field profiles, extracted from the reflectance simulation, show a redistribution of the electric field toward the top corner. The grating is much more symmetric allowing the increase of the direct path through the grating.

Some differences exist between FDTD simulation and experimental data. First, we observe a blue shift of the spectra for the sample before regrowth in Fig. 6(a) compare to the experimental spectra (Fig. 5). This blue shift is probably due to the dimension reduction of the ribbons after the regrowth because of the cleaning process and substrate preparation during the regrowth. In other words, the ribbons size is probably larger for sample B than for sample C. During the FDTD simulation, we kept constant the dimension and shape for the ribbons before and after the regrowth. Second, we do not observe the fourth mode at  $0.15 \mu\text{m}^{-1}$  (Fig. 5). Finally, the weak difference between FDTD model and experiments are probably due to imperfection of the geometry of the real structure, imperfection of the Drude model and inaccuracy of the index of the GaSb material (constant refractive index in the whole spectral range of simulation).

## 6. Conclusion

We have demonstrated that it is possible to integrate plasmonic arrays into a GaSb substrate by epitaxial regrowth after the plasmonic device technology. This is a prerequisite for the development of all-semiconductor plasmonics based on antimony material. The excellent crystal quality of the regrown material opens the possibility to integrate plasmonic functionalities at the heart of photonic devices. The embedded arrays exhibit asymmetric Fano-like line shapes which are due to interferences between the direct transmitted light through the array which can be viewed as a homogenized material and the light scattered by the plasmonic resonator. This work paves the way to all-semiconductor plasmonics for mid-IR photonic applications.

## Acknowledgment

This work was partially funded by the French “Investment for the Future” program (EquipEx EXTRA, ANR 11-EQPX-0016), and by the French ANR (SUPREME-B, ANR-14-CE26-0015). Eric Tournié gratefully acknowledges support from Institut Universitaire de France (IUF).